nature climate change

SUPPLEMENTARY INFORMATION

DOI: 10.1038/NCLIMATE2471

Flood risk of natural and embanked landscapes on the Ganges–Brahmaputra tidal delta plain

L. W. Auerbach[1], S. L. Goodbred Jr[1]*, D. R. Mondal[2], C. A. Wilson[1], K. R. Ahmed[3], K. Roy[3], M. S. Steckler[4], C. Small[4], J. M. Gilligan[1], B. A. Ackerly[5]

[1]Deptartment of Earth and Environmental Sciences, Vanderbilt University, Nashville, Tennessee 37240, USA. [2]School of Earth and Environmental Sciences, Queens College - City University of New York, Queens, NY 11367, USA. [3]Environmental Science Discipline, Khulna University, Khulna, Bangladesh 9208. [4]Lamont-Doherty Earth Observatory, Columbia University, Palisades, NY 10964, USA. [5]Department of Political Science, Vanderbilt University, Nashville, TN 37203, USA. *email: steven.goodbred@vanderbilt.edu

1. Shuttle Radar Topography Mission (SRTM) Elevation Data

SRTM elevation data for the lower G-B delta demonstrate that results and conclusions drawn from this study regarding local landscape elevations can be generalized beyond Polder 32, specifically to the southwestern region of Bangladesh (Supplementary Fig. 1). For these poldered regions, including Polder 32, historical deforestation and widespread conversion to agriculture account for the SRTM data reflecting actual land-surface elevations, not tree tops or structural artifacts. The resulting patterns demonstrate that much of the poldered region lies ≤1.5 m relative to the EGM96 datum, which is consistent with the GPS elevation data collected for this study on Polder 32 (Supplementary Fig. 1). General conclusions about the Sundarbans region are more difficult to assess due to elevations reflecting tree canopy height, not land surface elevation. However, the presence of a dense, consistent vegetation canopy reflects that the land surface is in relative equilibrium within the narrow range of floral tolerance to inundation.

2. Embankment Breach Locations on Polder 32

From 2001 to 2011, 50-200 m of bank erosion is documented along the west and northwest margins of the polder (Supplementary Fig. 8b,d). Bathymetric surveys reveal that the channel thalweg (deepest point) at these sites lies at the base of the eroding shoreline, typical of cut-bank morphology (Supplementary Fig. 8a,c). These patterns suggest that undercutting or oversteepening are likely to be factors in the embankment failures. Significant channel meandering is evident at two of the five breach locations, with notable point-bar development and cut-bank erosion in the decade prior to embankment breaches. Four of the five breaches also occurred at the mouths of former tidal channels blocked by the embankments and scoured into sand following the failures, suggesting that hydrostatic forces acting upon shallow subsurface sands may have played a role in some of the embankment failures (Fig. 1).

Furthermore, Polder 32 lies at the transition from the natural Sundarbans to the poldered landscape, where the force of the storm surge may have been locally intensified as flood waters moved from the unrestricted tidal channels of the Sundarbans to the highly restricted channels of

the embanked region. Given the modest storm surge height (Supplementary Fig. 3; ~0.5 m above spring high tide), it is also likely that the out-of-phase timing between the flooding storm surge and ebbing astronomical tide generated locally accelerated current velocities and scour within existing channel thalwegs. In summary we note that the preferential failure of embankments at Polder 32 and at specific locations on the island were non-randomly distributed and clearly correlate with the physical attributes described above; however, the exact cause or combination of factors causing the failures remains uncertain.

3. Tidal Splay Deposits

Sediment cores collected on Polder 32 revealed a locally thick, surficial deposit of silt and fine-sand laminae at 67 of 114 sampled locations (Figs. 1, 3d and Supplementary Fig. 10). These deposits range in thickness from 10- cm to 72 cm (Supplementary Fig. 11), with a mean of 40 cm, and were most apparent as tidal splay deposits located adjacent to large channel scours observable in post-storm satellite imagery (Fig. 1). The well-laminated sandy unit is consistently underlain by a darker grey, silty soil that corresponds to the former agricultural surface prior to flooding (Supplementary Fig. 10). We infer that the tidal splay deposits are a product of the two-year period of daily tidal inundation that followed embankment breaches. Areas of Polder 32 that did not experience significant post-storm deposition were generally located at the distal reaches of the tidal splay features or where local embankments were repaired soon after the storm. By contrast, Polders 31 and 33 to the west and east of Polder 32, respectively, were subjected to only local flooding during the storm and none thereafter (Fig. 1). At these locations, 7 of 11 sediment cores comprised only the ambient agricultural soil, with the remaining sites bearing just a few centimeters of storm-deposited sediment.

4. Compaction and Wood Extraction Estimates

Compaction in coastal deltas, which may be a great source of elevation offset, is perhaps the least constrained parameter for a land surface budget, particularly in the G-B delta. In a global assessment of deltas, ref. 1 differentiated compaction due to natural processes (C_n = loss in void space due dewatering, grain packing realignment, also oxidation of organic matter) and anthropogenic compaction (C_a = volume change from underground [oil, gas, water] extraction, human-influenced soil drainage and accelerated oxidation). In the G-B delta, natural compaction is likely to be spatially and temporally variable, depending on heterogeneous stratigraphy; however no substantive measurements of natural compaction have been reported to date. Recent preliminary results from fiber-optic cables installed at different locations in the G-B delta indicate compaction may be confined to the upper 10 m of sediment (S. Nooner [U. of North Carolina, Wilmington] and M. Steckler [Columbia U.], personal communication). We estimate a conservative value of 0.4 cm/yr for C_n, which is similar to that reported for coastal Bangladesh[2] and would be the only source of compaction affecting the 'pristine' Sundarbans landscape. Local observations indicate that saline groundwaters in the region preclude extraction for irrigation or household consumption, so this potential source of compaction is not relevant in most of SW Bangladesh. However, due to substantial human-modification to the poldered landscape, including draining of surface water and soils for agriculture, we expect C_a to be more significant in populated regions of the G-B delta. Therefore, we estimate an enhanced rate of shallow soil compaction of 0.8 cm/yr for poldered areas to account for these processes (Supplementary Fig. 12). This value is expected to be a short-term consequence of the initial draining and drying of

shallow (<5 m) sediments following embankment construction, and not necessarily a rate that persists for the next century.

Loss of belowground biomass (e.g., oxidation or removal of roots, peat) can have also a considerable effect on delta evolution. Since poldered areas were once forested mangrove, we assume that belowground volume taken up by trunks and roots would have been lost through oxidation upon drying of the soils and/or direct extraction for fuel, which is a regular practice today. To estimate the impact of deforestation on belowground biomass, we have used field observations (Supplementary Table 1) and the equation established by ref. 3 to calculate a net elevation loss of ~ 20 cm associated with biomass loss and wood extraction. Because this deforestation would likely have occurred relatively quickly after embankment construction (within a few years to decades), we consider this 20-cm elevation loss as a "single event," as opposed to a persistent rate over the 50 years since poldering. This magnitude of elevation loss associated with belowground root oxidation is comparable to modeled mangrove peat collapse in Honduras after Hurricane Mitch (13 cm in 10 years; ref. 4). We concede that the aforementioned rates are first-order estimates but consider them to provide reasonable constraints on the contribution of wood extraction to the observed elevation offsets.

References

1. Syvitski, J. P. M. *et al.* Sinking deltas due to human activities. *Nat. Geosci.* **2,** 681–686 (2009).

2. Stanley, D. J. & Hait, A. K. Holocene depositional patterns, neotectonics, and Sundarban mangroves in the western Ganges-Brahmaputra delta. *J. Coast. Res.* **16,** 26–39 (2000).

3. Komiyama, A., Poungparn, S. & Kato, S. Common allometric equations for estimating the tree weight of mangroves. *J. Trop. Ecol.* **21,** 471–477 (2005).

4. Cahoon, D. R. *et al.* Mass tree mortality leads to mangrove peat collapse at Bay Islands, Honduras after Hurricane Mitch. *Ecology* **91,** 1093–1105 (2003).

5. Razzaque, M. A. *Chemical pulping and wallboard experiments with sundri (Heritiera minor) wood. Forest Products Laboratory (U.S.) Report no.2253*. (1962).

Table S1 | Root volume calculations from five species of mangroves in the Sundarbans.

Tree species	dbh (cm)	dbh^2 (cm^2)	W_R (kg)	W_v (m^3)
Sundri	51	2601	1268	1.2
Heritiera fomes (ref. 5)	79	6241	3350	3.2
ρ = 0.97 t/m^3 to 1.1 t/m^3	78	6084	3256	3.1
	45	2061	979	0.9
	68	4624	2401	2.3
	54	2916	1440	1.4
	49	2401	1160	1.1
Cedar Mangrove (*Passur*)	122	14884	5384	9.0
Xylocarpus mekongensis (ref. 3)	156	24398	9319	15.5
ρ = ~0.6 t/m^3	92	8464	2878	4.8
	143	20449	7661	12.8
	66	4356	1377	2.3
	99	9801	3386	5.6
	49	2401	711	1.2
	110	12100	4279	7.1
	75	5625	1828	3.0
	129	16641	6094	10.2
	145	21025	7900	13.2
	163	26569	10244	17.1
	84	7056	2351	3.9
	115	13225	4722	7.9
	87	7569	2542	4.2
	93	8649	2947	4.9
	76	5776	1883	3.1
	81	6561	2169	3.6
	72	5184	1670	2.8
White/Grey Mangrove (*Baen*)	248	61901	26193	43.7
Avicennia sp. (ref. 3)	121	14641	5287	8.8
ρ = ~0.6 t/m^3	135	18225	6741	11.2
	92	8464	2878	4.8
	109	11881	4193	7.0
	102	10404	3618	6.0
	134	17956	6631	11.1
Large-leaf Orange Mangrove (*Kankra*)	103	10609	4242	6.1
Bruguiera gymnorrhiza (ref. 3)	80	6400	2421	3.5
ρ = ~0.7 t/m^3	62	3844	1375	2.0
Mangrove Apple (*Keora*)	172	29584	11542	19.2
Sonneratia apetala (ref. 3)	147	21609	8144	13.6
ρ = ~0.6 t/m^3	110	12100	4279	7.1
	142	20164	7542	12.6

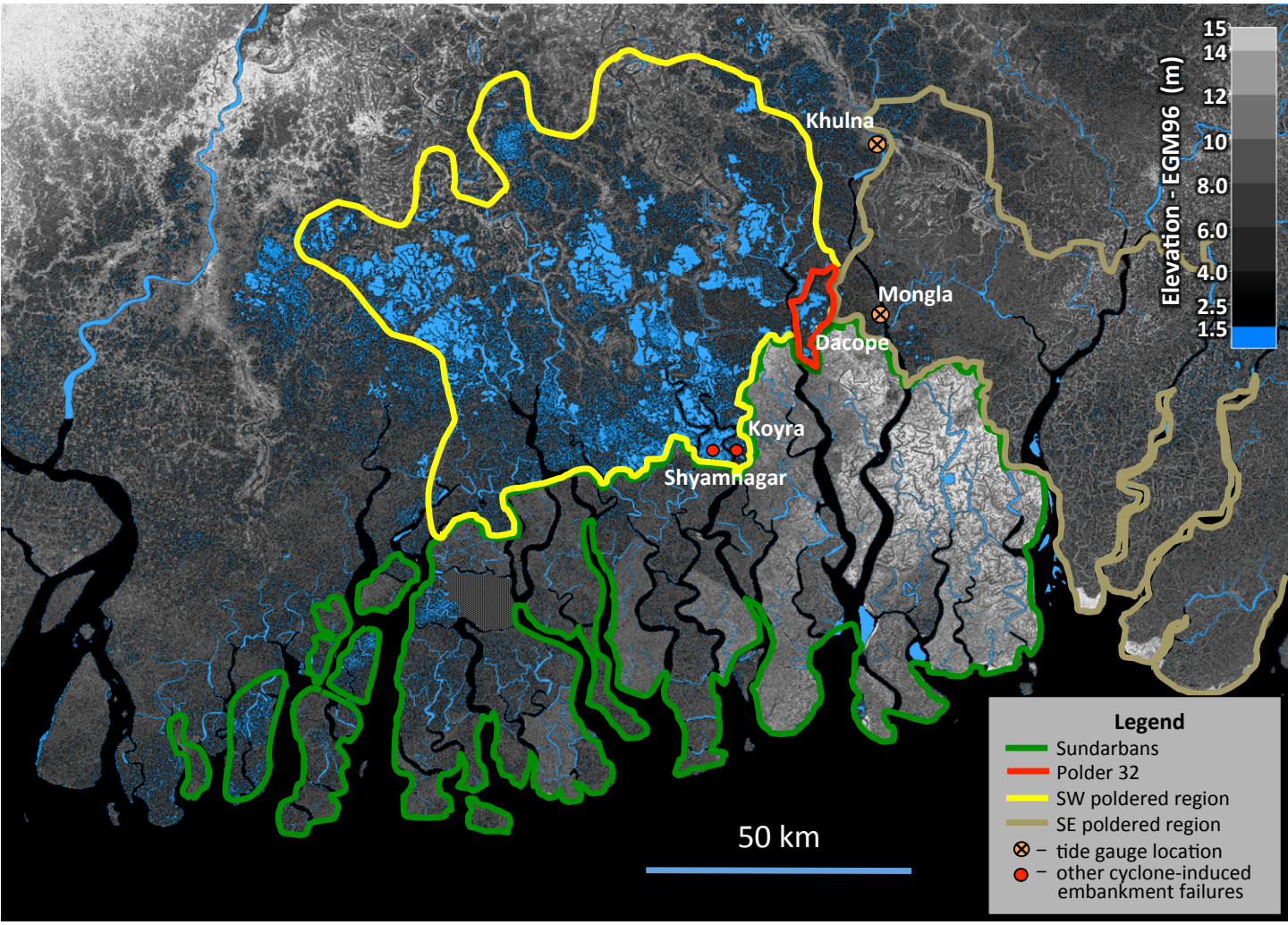

Figure S1 | Digital Elevation Model of the lower Ganges-Brahmaputra delta. SRTM elevation data show that much of the inland southwest (SW) poldered region is positioned below 1.5 m relative to EGM96, placing it ≥1 m below local mean high water and susceptible to severe tidal flooding in the absence of embankment protection (Fig. 2). Koyra, Shymnagar, and Polder 32 in Dacope each experienced major embankment breaches during Cyclone Aila and suffered months to years of tidal inundation before embankment repair. In contrast, embanked landscapes in the southeastern (SE) polders are younger landscape and positioned at higher elevation. Although susceptible to temporary storm-surge flooding, the SE region is generally less susceptible to sustained flooding by tides due to its higher elevation. The Sundarban mangrove forest appears as a relatively high area due to dense natural tree canopy. However, the Sundarbans landscape is naturally flooded by tidal waters, supporting regular sedimentation and maintenance of its elevation. The Sundarbans flood primarily on spring high tides and for relative short durations (2-4 hrs/day).

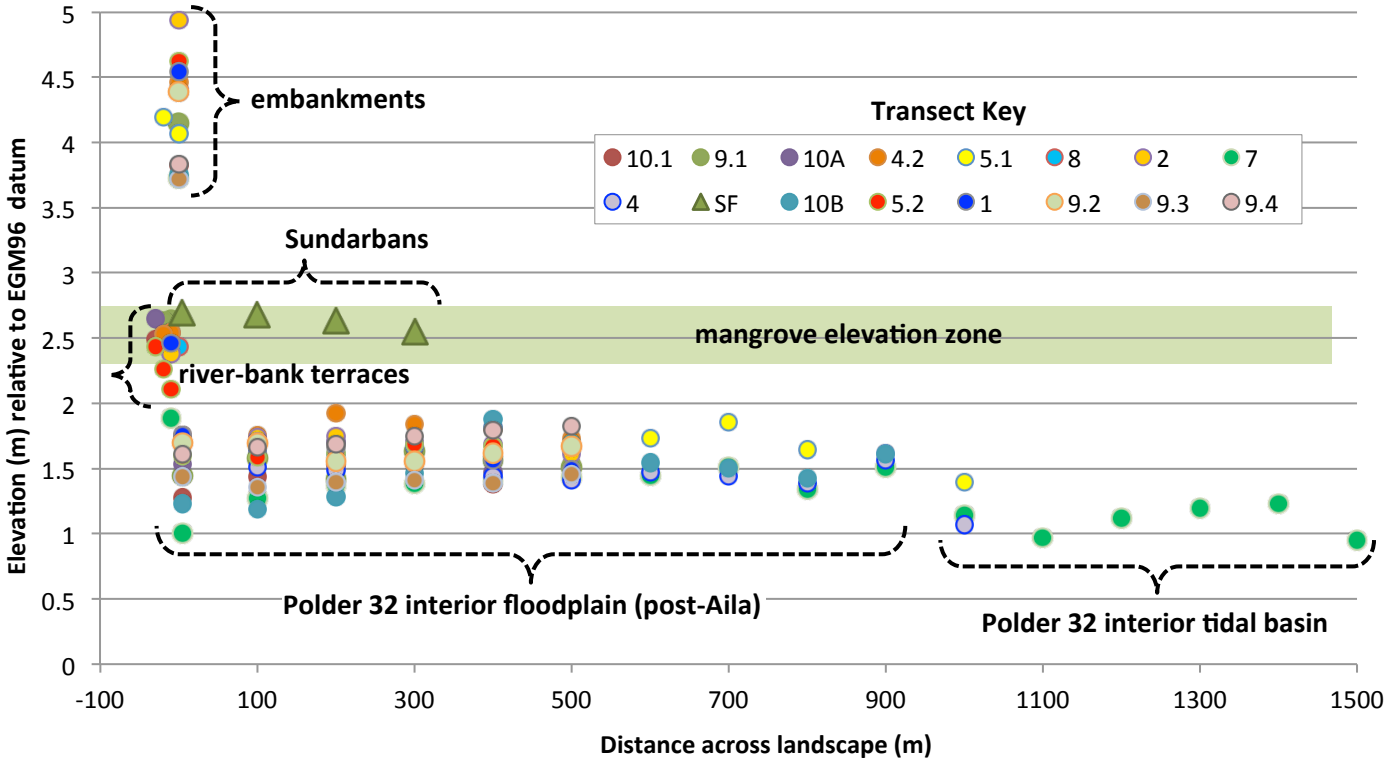

Figure S2 | GPS elevation survey data. Polder 32 elevation transects (colored circles) extend up to 1500 m from the embankment into the polder interior. These results are the same dataset shown in Figure 2, but here the full data range of transect >500 m inland of the embankments are shown. Mean elevation of the polder interior floodplain is 1.5±0.1 m, with its protective embankments ranging 3.7 to 4.6±0.1 m. The mean elevation of the Sundarbans (green triangles) is 2.65±0.10 m, with the range of intertidal mangrove vegetation shown by the green bar.

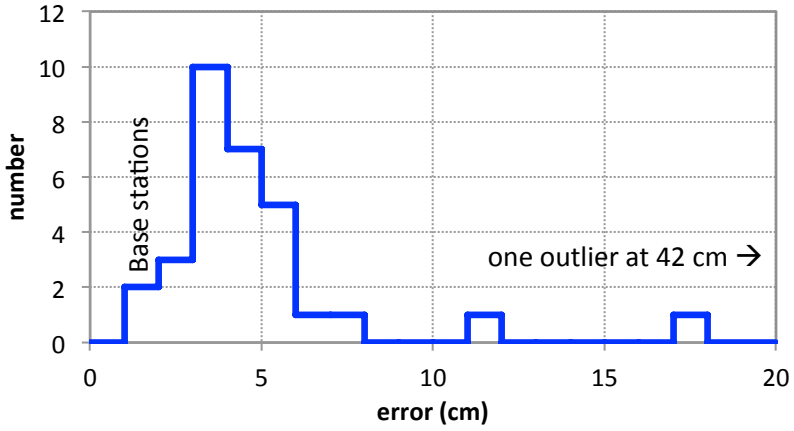

Figure S3 | Histogram of error for the GPS elevations. Mean error of the dataset is 5.2±2.8 cm.

Figure S4 | Plot of GPS survey point locations with symbols proportional to their elevation error, ranging 2-42 cm.

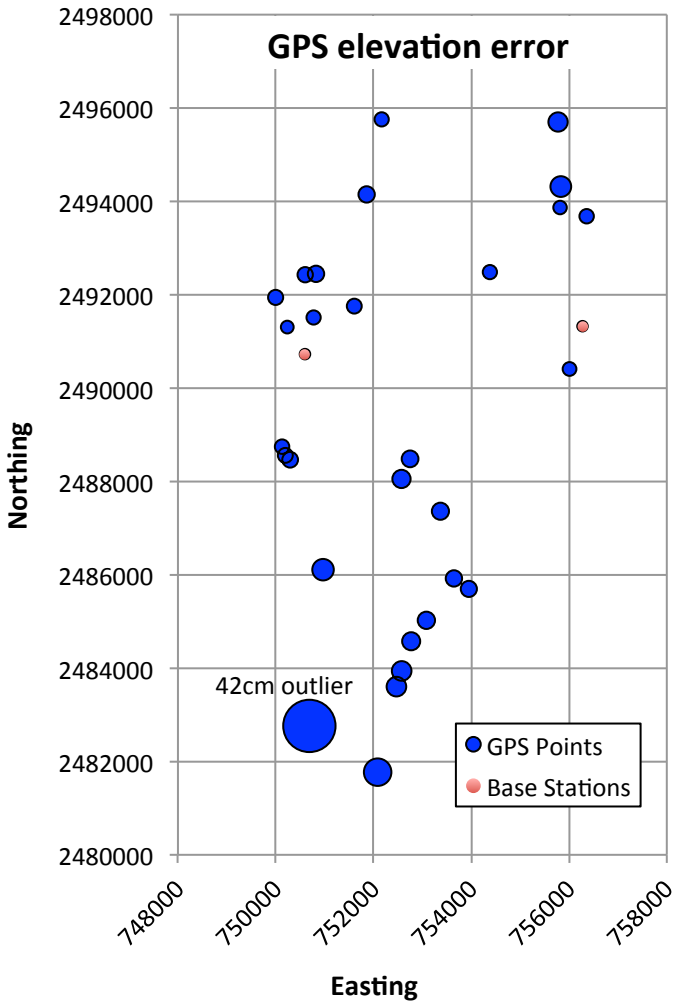

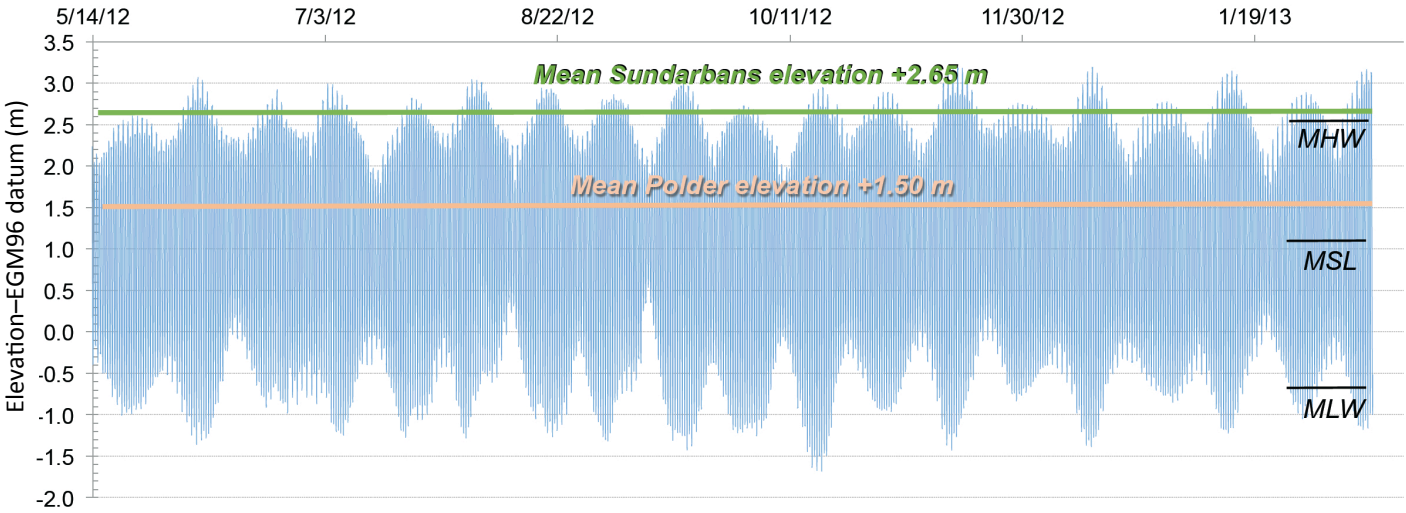

Figure S5 | Water-level data from tidal channel east of Polder 32. Data collected at 10-minute intervals using a deployed pressure gauge. Location shown in Figure 1. Instrument height was surveyed during the GPS survey to tie observed water levels to the EGM96 datum. The characteristic fortnightly variations in tidal range reflect spring-neap astronomical cycles.

Figure S6 | Field photos contrasting tidal channel water levels with Polder 32 interior. a, b Photos of newly reconstructed embankment along one of the major breaches. Images taken near to spring high tide, contrasting the relative elevation between high water and the polder interior.

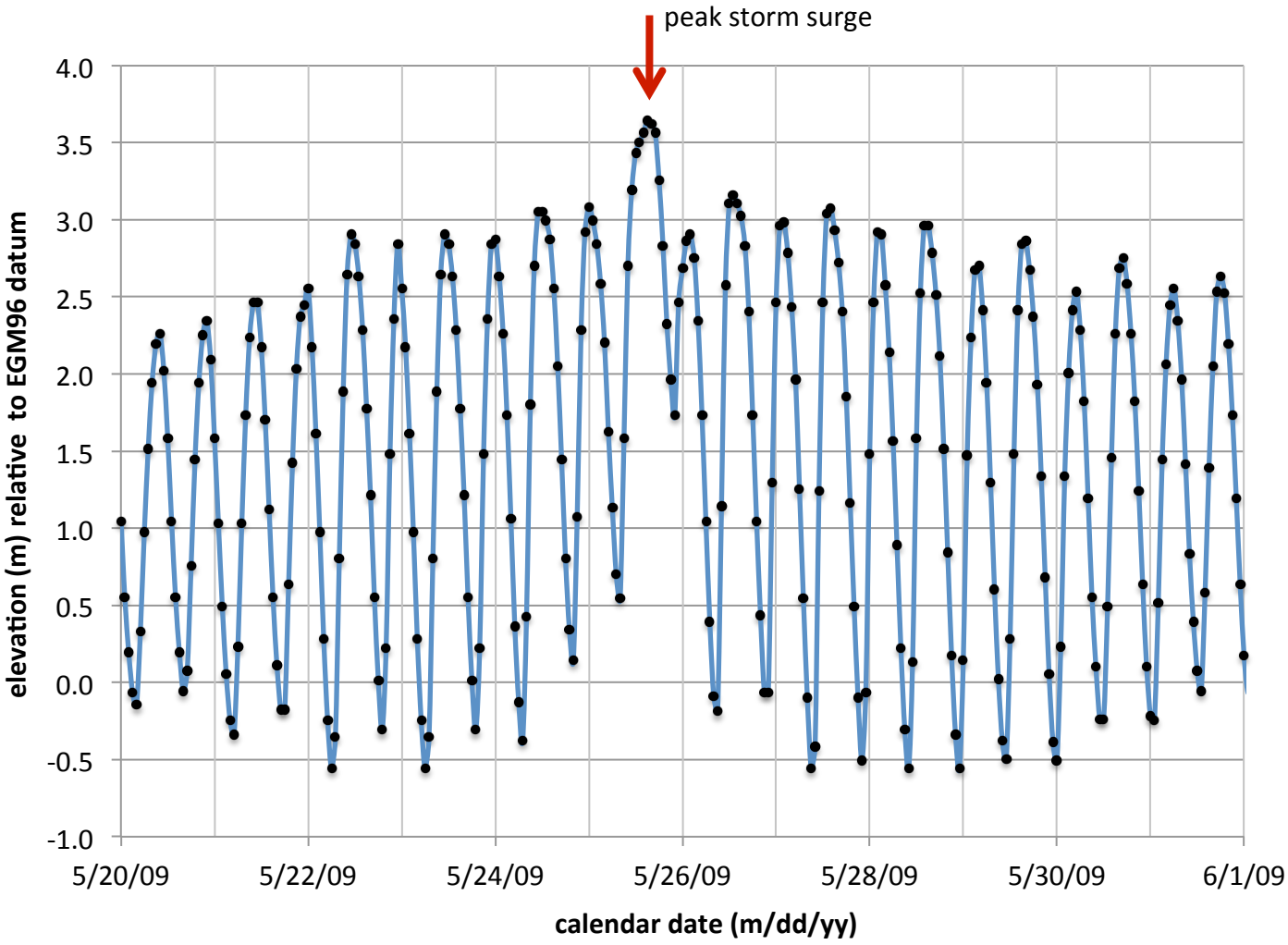

Figure S7 |Tide gauge record showing Cyclone Aila storm surge. The storm made landfall on May 25, 2009, coinciding with low tide. With much of the storm inland during the ensuing flood tide, the resulting surge (red arrow) was only ~50 cm above the astronomical high tide. There were no reports of the surge overtopping the embankments on Polder 32, yet the storm forced five major breaches of the embankments despite the modest surge height (Figure 1). The tide gauge data shown here are from Mongla, about 15 km east of Polder 32 (Figure S1) and connected by several large tidal channels .

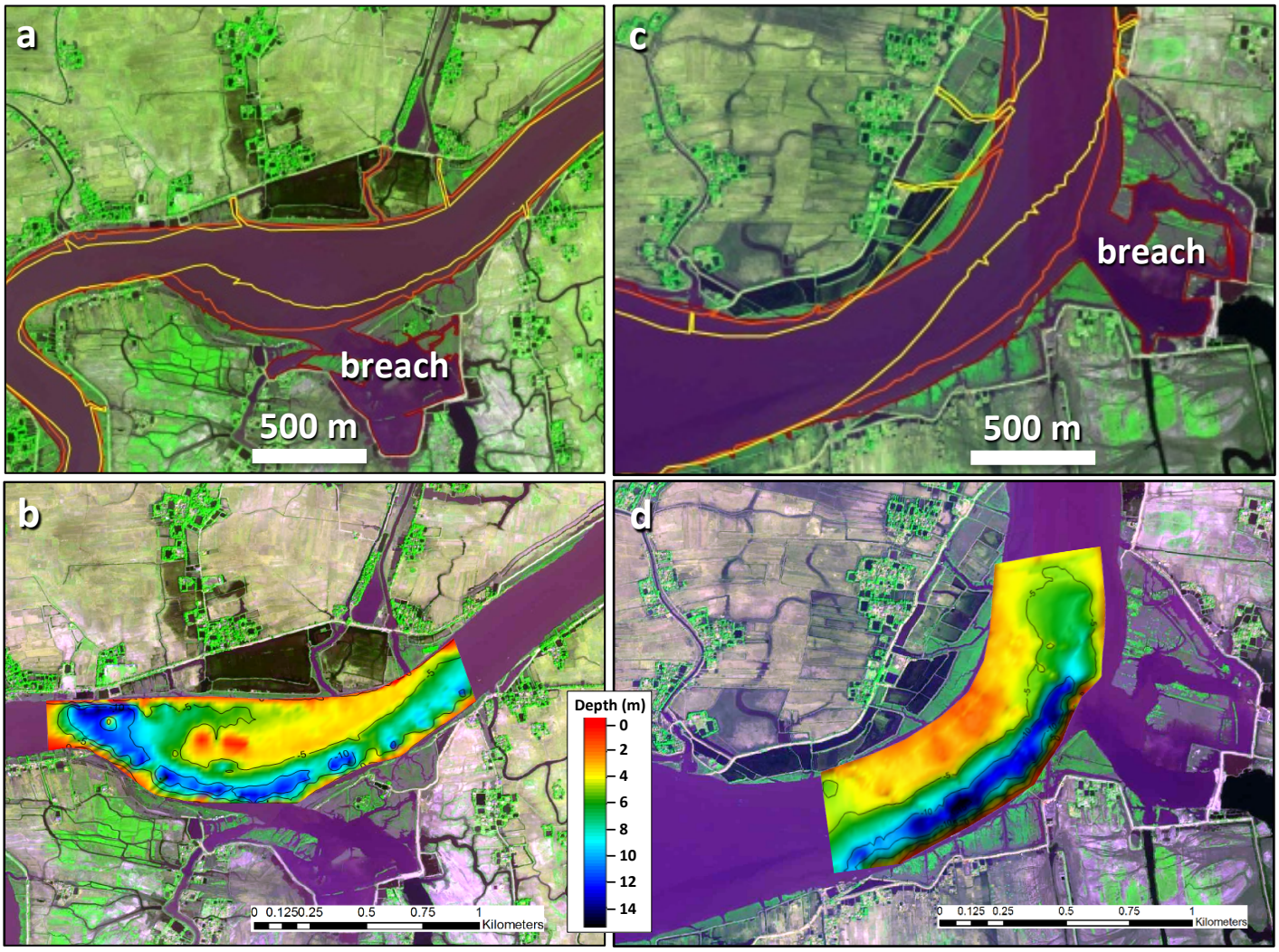

Figure S8 |Paired images showing bank migration and bathymetry of the river channels at two breach locations on Polder 32. Locations in Figure 1; basemap courtesy of DigitalGlobe©. **a**, **c,** Bankline changes from 2001 (yellow) to 2009 just before Cyclone Aila (orange) show tens to hundreds of meters of shoreline erosion that had forced previous reconstruction of the embankments at these locations. The 2012 post-Aila bankline position is shown in red. **b, d,** Bathymetric survey data from this study showing the channel thalweg positioned at the sites of maximum erosion over the previous decade and where the embankments failed during Aila.

Figure S9 | Field photos showing embankments and repair efforts on Polder 32. **a,** Local and regional labor reconstructing a portion of embankment. Concrete blocks are made on site and emplaced by hand. Embankment repair and maintenance was an important income source following Cyclone Aila during the temporary loss of local livelihoods such as shrimping and rice cultivation. Photos taken at low tide. **b,** Repaired sections of the Polder 32 embankment observed along the Sibsa River during high tide.

Figure S10 | Photo of sediment core showing silt and fine sand tidal laminites deposited during 18-24 months of post-Aila tidal inundation. The deposit at this site is 40-cm thick and overlies the gray, reducing soil horizon that defines the pre-cyclone agricultural surface.

Figure S11 | Histogram of tidal-splay sediment thickness measured across Polder 32. Post-storm tidal sediments were identified in 67 of 114 cores, ranging in thickness from 5-72 cm. Mean measured thickness of deposited sediment is 37±18 cm.

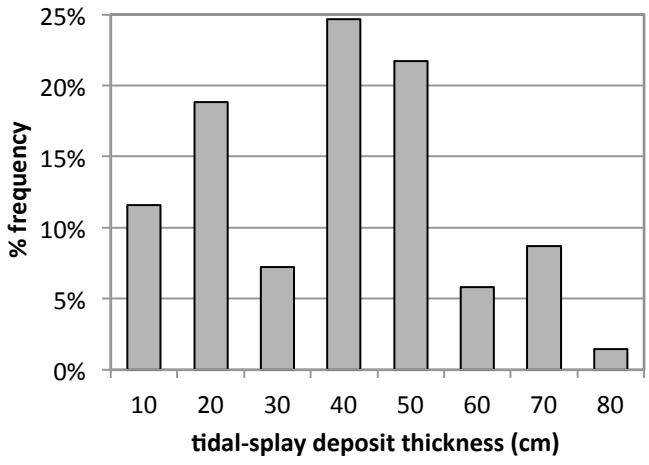

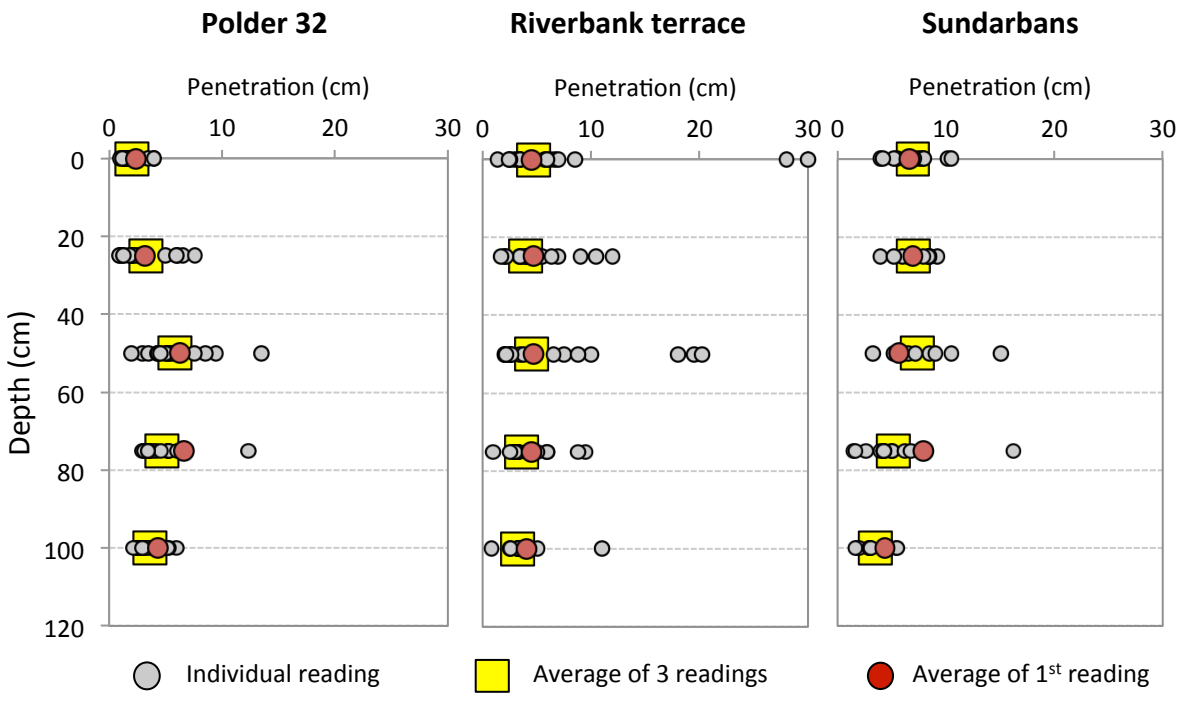

Figure S12 | Results of dynamic cone penetrometer tests. Results show that sediments in the upper 50 cm on Polder 32 are more consolidated than sediments on the riverbank terraces and in the Sundarbans.